




Article

Torque Allocation of Hybrid Electric Trucks for Drivability and Transient Emissions Reduction

Luca Dimauro , Antonio Tota , Enrico Galvagno  and Mauro Velardocchia *

Department of Mechanical and Aerospace Engineering, Politecnico di Torino, Corso Duca Degli Abruzzi 24, 10129 Torino, Italy

* Correspondence: mauro.velardocchia@polito.it

Abstract: This paper aims at investigating powertrain behaviour, especially in transient dynamic responses, using a nonlinear truck vehicle dynamic model with a parallel hybrid configuration. A power split control was designed to achieve the desired drivability performance, with a focus on NOx emissions. The controller was characterized by high-level model-based logic used to elaborate the total powertrain torque required, and a low-level allocation strategy for splitting power between the engine and the electric motor. The final task was to enhance vehicle drivability based on driver requests, with the goal of reducing—in a hybrid configuration—transient diesel engine emissions when compared to a conventional pure thermal engine powertrain. Different parameters were investigated for the assessment of powertrain performance, in terms of external input disturbance rejection and NOx emissions reduction. The investigation of torque allocation performance was limited to the simulation of a Tip-in manoeuvre, which showed a satisfying trade-off between vehicle drivability and transient emissions.

Keywords: parallel hybrid truck vehicle model; NOx emissions; torque allocation control logic; phlegmatization; drivability and emission trade-off



Citation: Dimauro, L.; Tota, A.; Galvagno, E.; Velardocchia, M.

Torque Allocation of Hybrid Electric Trucks for Drivability and Transient Emissions Reduction. *Appl. Sci.* **2023**, *13*, 3704. <https://doi.org/10.3390/app13063704>

Academic Editors: Vincenzo Di Dio, Antonella Castellano and Marco Cammalleri

Received: 22 February 2023

Revised: 8 March 2023

Accepted: 9 March 2023

Published: 14 March 2023



Copyright: © 2023 by the authors. Licensee MDPI, Basel, Switzerland. This article is an open access article distributed under the terms and conditions of the Creative Commons Attribution (CC BY) license (<https://creativecommons.org/licenses/by/4.0/>).

1. Introduction

In recent years, an ever-increasing number of researchers have focused their efforts on the substantial challenge of powertrain electrification in an attempt to deal with new government requirements that aim at reducing pollutant emissions and fuel consumption [1]. In this context, the Research and Development (R&D) departments of several automobile companies are engaged in the development of innovative powertrain solutions to replace vehicles with fuel motorization. A slow and progressive transition from internal combustion engine vehicles (ICEVs) to zero emissions vehicles (ZEVs), battery electric vehicles (BEVs), and fuel cell electric vehicles (FCEVs) is occurring, along with the development of hybrid electric vehicles (HEVs) and plug-in hybrid electric vehicles (PHEVs).

As proposed in [2], several possible topological architectures can be implemented in HEVs, where two or more sources of power/energy are combined to achieve the required power necessary to propel the vehicle. HEV vehicles combine the ICE power with an electric traction motor, which is powered by an energy storage device generally known as battery pack. The most common configurations adopted to couple different power sources can be summarized as parallel hybrid [3], series hybrid [4] or combined series–parallel architectures, with a mechanical power-split [5–8] or innovative magnetic split [9]. Different control strategies have been investigated and proposed to achieve optimal energy management [10] between different power sources. HEVs combine the advantages of electric motor drives—having quick acceleration—with good ICE performance at constant speeds. On the other hand, vehicle drivability [11] is highly affected, as during rapid torque transients—due to drivers' abrupt accelerations—noise and vibrations [12] can occur during engine start/stop conditions [13] in mild hybrid electric vehicles.

Besides this aspect, sudden driver torque requests can generate an increase in NO_x emissions, as investigated in [14] during tip-in/tip-out manoeuvres. Hence, control strategies should act in a multiphysics way, also considering—besides optimal energy management—NO_x and CO₂ emissions [15] and, more generally, the reduction of pollutant emissions into the environment [16].

The aim of this paper is to address the topics of both drivability enhancement and the reduction of pollutant emissions; thus, the development of a vehicle model that is able to predict and highlight all these aspects is required—as carried out in [17], where Gear Shift Patterns were optimized to fulfil multiple constraints in terms of customer requirements such as drivability, NVH performance, emissions, and fuel consumption. These last two aspects were considered in [18] to evaluate fuel savings and NO_x benefits when predictive control is applied to a mild hybrid truck, using dynamic programming with backtracking. Conversely, [19] proposed a novel real-time Energy Management Strategy (EMS) that was integrated with a model to use physical considerations to estimate energy consumption during gearshifts in Dual-Clutch Transmissions (DCT).

The development of a transmission model with a high level of accuracy is necessary to describe the dynamic behaviour of the whole system well, although its complexity can be reduced with appropriate simplifications—as carried out in [20] with a hybrid model of a vehicle driveline that was partially lumped and partially distributed to investigate vibrational phenomena inside the transmissions known as “shuffle” and “clonk”. A methodology for the evaluation of clunking noises during gearshifts was also proposed in [21] using a nonlinear lumped parameter model of DCT, developed in an Amesim environment, while a Matlab/Simulink environment was adopted in [22] for the evaluation of NVH performance in the DCT transmission of a C-segment passenger car. Coming back to hybrid vehicles, mathematical models of both conventional and mild hybrid powertrain were developed in [23] through the integration of a conventional manual transmission-equipped powertrain and an electric motor as a secondary power source, in order to study the performance of partial power-on gear shifts through the implementation of torque hole-filling by the electric motor during gearshifts.

Besides the modelling of mechanical components, an appropriate tyre model can have relevant effects on simulated dynamics, as they have also a considerable influence on damping effects inside the powertrain. [24] demonstrated, using appropriate identification techniques aimed at describing tyre torsional dynamics in the frequency range 10–50 Hz, that damping is more accurately represented if modelled as hysteretic and not as viscous when the tyre load is low. Conversely, [25] proposed three different tyre models, e.g., modelled as a simple torsional spring, adopting a linear slip model, or assuming a fixed relaxation length; these last two models introduced nonlinearity, as an instantaneous slip ratio was considered. The relaxation length was estimated from the steady state tyre properties in [26] and included wheel load and slip dependencies. The adoption of this parameter is necessary for the description of interactions between tyres and roads, as all the other chassis components influence vehicle dynamic properties through tyre contact forces and torques.

A lumped LuGre tyre ground contact model was modelled in [27] and in [28], where the developed dynamic friction tyre model was able to accurately capture the transient behaviour of the friction force observed during transitions between braking and acceleration phases. Other researchers have instead used software for tyre dynamics to compute the forces acting on the tyre and hence on the steel wheel for other purposes, such as fatigue assessment [29].

The parallel mild hybrid architecture of a heavy commercial vehicle developed for this research study is similar to the one adopted in [30], but with the improvement of implementing three different control strategies for the direct control of vehicle acceleration, vehicle speed control, and torque control, with superposed active damping of drive train oscillations. The torque distribution between the two power sources is managed as a different task from the regulation task (oscillation damping), adopting a specific control

algorithm that does not require the implementation of an optimisation problem. Moreover, as regards the linear model used for the design of the controller, an accurate tyre model with a fixed relaxation length is adopted—thus decoupling the kinematic behaviour of the driving rear tyres from the free rolling condition, as carried out in [25].

The developed model should also be able to reduce drivetrain vibrations; different works addressing this aim can be found in literature. In [31], a control for vibration reduction was developed for hybrid vehicles and experimentally validated, with two different controllers that reduced both the vibrations due to engine torque ripple and ones related to the driveline. Conversely, the root locus technique [32] has been adopted for anti-jerk control designs capable of preserving the driveline from oscillations. To improve NVH performance, a magnetic differential for vehicle drivetrains was developed in [33], while a controller for driving the engine—in order to actively damp driveline oscillations—was proposed in [34] to improve drivability and passenger comfort.

The present paper aims to propose an accurate nonlinear vehicle model and a model-based torque allocation control to achieve both improved vehicle drivability and pollutant emissions performance. The controller is designed in two steps with different aims: high-level logic was used in order to aim at providing a total powertrain torque able to satisfy the desired drivability performance in terms of longitudinal acceleration dynamics, through the integration of a direct feedforward term with a feedback contribution designed based on the Linear Quadratic Regulator (LQR) theory [35–37]; meanwhile, the low-level control allocation is designed to split the torque between the engine and the electric motor for emissions reduction purposes. The main contribution of the paper is to:

- propose a nonlinear dynamic model that considers the main vehicle nonlinearities, e.g., the elastic and damping behaviour of the torsional damper and the transient model of the tyres' dynamics—thus representing a reference model for vehicle performance assessment and torque controller validation;
- show the benefits introduced by the proposed controller in terms of dynamic performance, driveline oscillations, and NO_x emissions;
- test the controller's robustness against the presence of unpredictable external inputs, e.g., a sudden road slope.

The paper is organised as follows: in Section 2 the nonlinear truck model—developed in a Matlab/Simulink environment—is shown and its characteristic dynamic equations are described, while in Section 3, the torque allocation control—based on the driver's intentions—is designed to reduce driveline oscillations and improve emissions performance. In Section 4, the controller performance is investigated to analyse the dynamic response of the powertrain and to evaluate the reduction of engine emissions. Finally, the conclusions of the work are discussed in Section 5.

2. Hybrid Vehicle Powertrain Layout

In this paper, a P0 mild parallel hybrid electric powertrain with a diesel engine was adopted. In this system architecture, better known as a belted alternator starter (BAS) [38,39], the internal combustion engine (ICE) and the electric motor (EM) are combined by means of a belt and work together to supply the necessary power to the vehicle. The EM is not able to propel the vehicle by itself; hence, it helps the ICE when extra power is required, behaving as a power booster [10]. With this configuration, an efficient engine start/stop functionality was ensured as well as the storage of energy in the battery during regenerative braking. Then, the power unit system was connected to the wheels through a gearbox and a differential.

The implementation of a parallel mild hybrid allowed us to benefit from the relevant advantages of the cooperation of EM and ICE, such as emissions reductions in case of slower transient behaviour in the ICE—better known as phlegmatization [40]—while the EM covered possible aggressive driver torque requests thanks to its high bandwidth—typical of electrical machines.

2.1. Matlab/Simulink Nonlinear Truck Model

The truck, shown in Figure 1, was modelled by means of a block-oriented approach [41,42], using a customized library of driveline components and adopting a user-friendly graphical interface—as shown in Figure 2. For each system component, it is necessary to define the dynamic laws by means of mechanical equilibrium principles, defining dynamic constants and constraints, and imposing the initial conditions. The input/output quantities of each component depend on the component topology. The Simulink model was grouped into subsystems, i.e., the engine, clutch damper, gearbox, differential, and wheels (2 driving and 2 driven), and a longitudinal truck vehicle model with longitudinal load transfer computation.

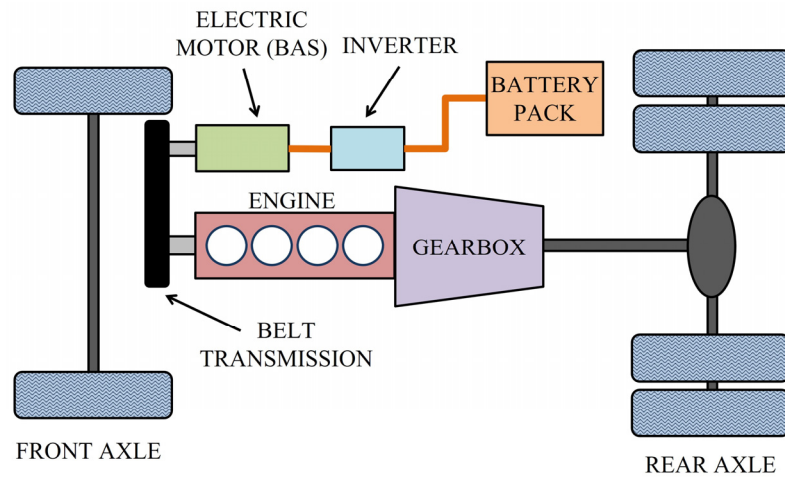


Figure 1. Transmission scheme of the parallel hybrid truck vehicle.

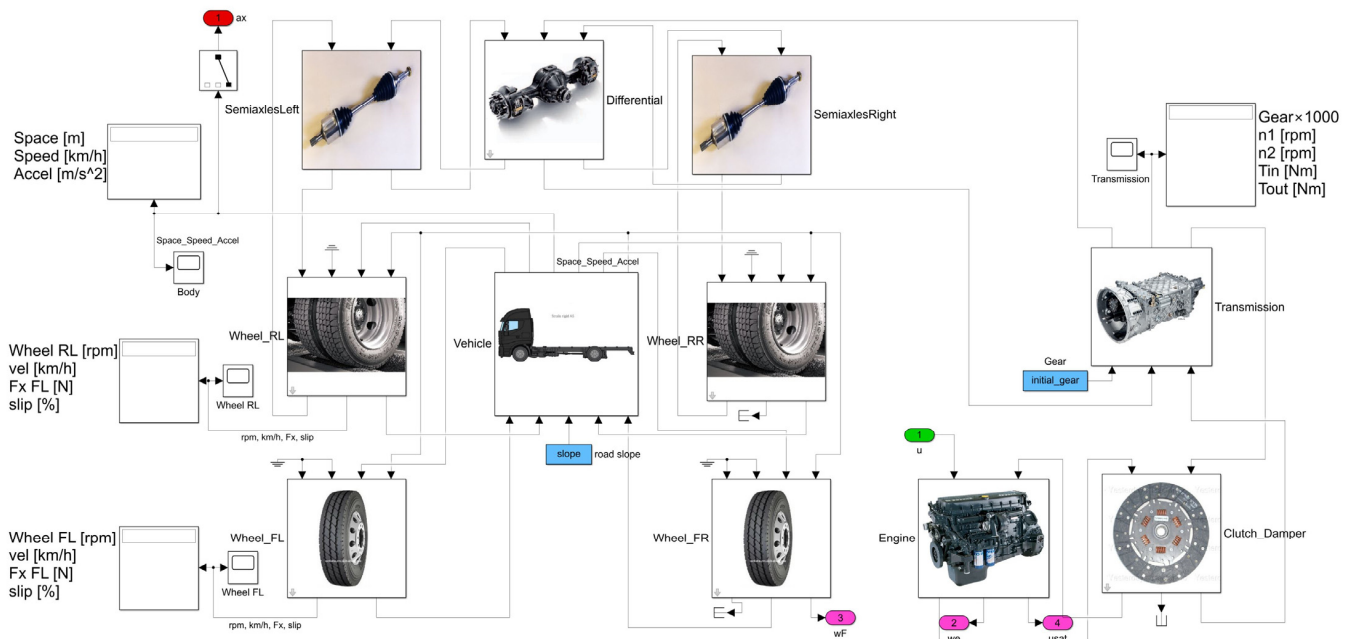


Figure 2. Nonlinear truck vehicle model in Matlab/Simulink environment.

Moreover, the model included the bi-linear elastic and damping behaviour of the torsional damper, the linear characteristic of the left and right-half shafts, a transient, nonlinear model for the tyres, and a Pacejka magic formulation [43] for road–tyre interactions.

Inside both the front and rear-tyre Simulink blocks, a wheel sensor was modelled, in order to apply a time delay and the effects of signal quantization to the simulated-wheel angular speed signal, to better reproduce experimental conditions.

2.2. Dynamic Equations

All the dynamic equations reported in this section are written in agreement with the free body diagrams of the drivetrain components and of the vehicle, which are reported in Figure 3.

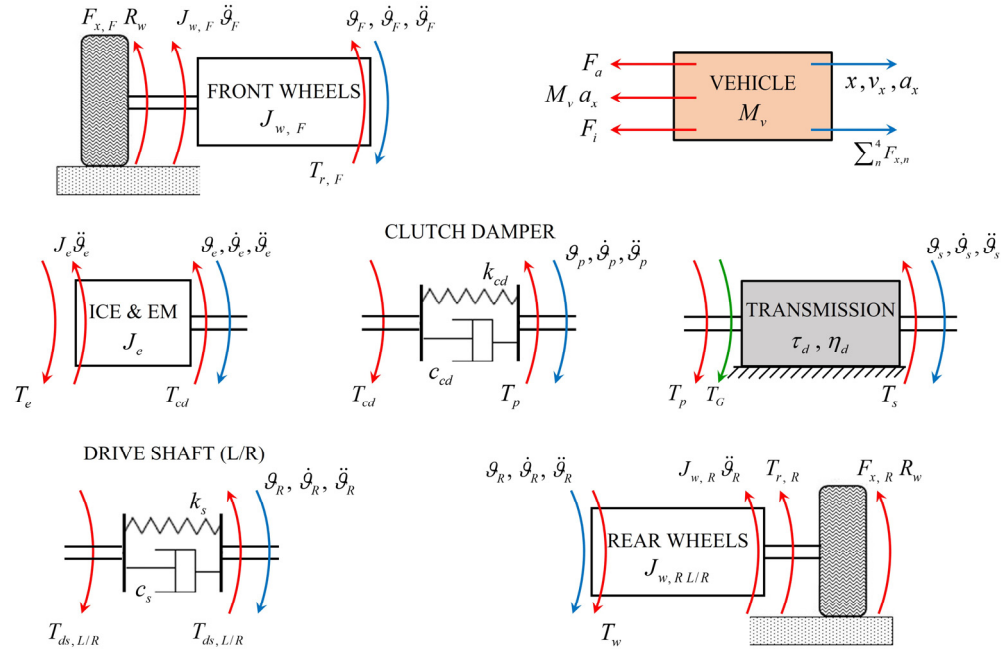


Figure 3. Free body diagrams of the main driveline components.

2.2.1. Power Source: ICE and EM

In the parallel hybrid configuration analysed, the ICE and the electric motor were connected by means of a belt, with a certain transmission ratio $\tau_b = \omega_{EM}/\omega_{ICE}$; hence, the total driving torque T_e , assuming 100% belt transmission efficiency, is given by:

$$T_e = T_{ICE} + T_{EM} \tau_b \tag{1}$$

The maximum torque of both the ICE and EM are reported in Figure 4. It is evident that the EM characteristic is symmetrical with respect to zero in case of traction or regenerative braking.

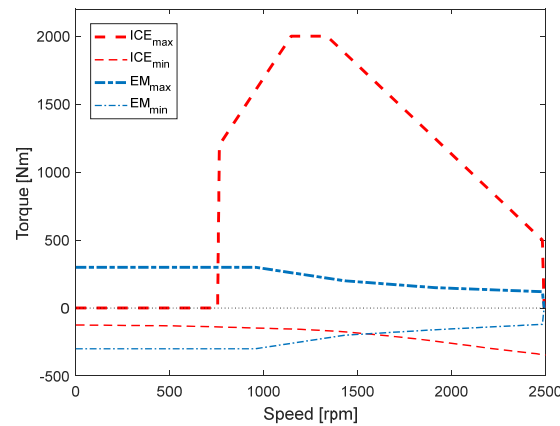


Figure 4. Torque characteristics of ICE and EM.

The acceleration of the engine $\ddot{\theta}_e$ was obtained from the equilibrium between the driving torque T_e , and the resistive torque of the primary shaft T_p , according to:

$$\ddot{\theta}_e = \frac{T_e - T_p}{J_e} \tag{2}$$

where J_e is the equivalent moment of inertia of the power source, so it depends on the ICE and EM inertias, which are related by the transmission ratio of the belted system as follows:

$$J_e = J_{ICE} + J_{EM} \tau_b^2 \tag{3}$$

2.2.2. Transmission: From Clutch Damper to Differential

The torque at the primary shaft T_p was obtained from the bi-linear clutch damper behaviour—whose nonlinear characteristics are reported in Figure 5—according to Equation (4):

$$T_p = T_{cd} = k_{cd}(\theta_e - \theta_p) + c_{cd}(\dot{\theta}_e - \dot{\theta}_p) \tag{4}$$

where k_{cd} and c_{cd} are the torsional stiffness and the torsional damping of the clutch damper, respectively.

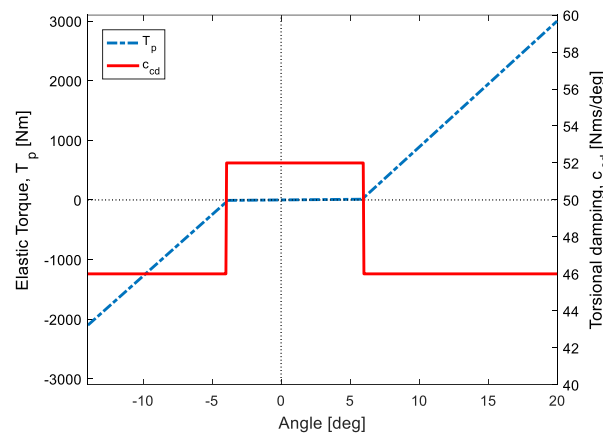


Figure 5. Elastic torque and viscous damping of the clutch damper.

The angular speed of the gearbox primary shaft $\dot{\theta}_p$ is related to the secondary shaft angular speed $\dot{\theta}_s$ by the kinematic relationship:

$$\dot{\theta}_p = \dot{\theta}_s \tau_d \tag{5}$$

where τ_d is the global driveline transmission ratio, depending on the actual gearbox gear ratio and the differential gear ratio, while the available torque at the secondary shaft—considering driveline efficiency η_d —is given by:

$$T_s = \eta_d \tau_d T_p = 2 T_{ds,L/R} = 2[k_s(\theta_s - \theta_R) + c_s(\dot{\theta}_s - \dot{\theta}_R)] \tag{6}$$

As reported in Equation (6), the drive shaft torque $T_{ds,L/R}$ was lumped using a viscous damper c_s and a torsional spring k_s . Instead, the torque $T_G = T_s - T_p$ corresponds to the torque supported by the gearbox constraints. Finally, torque dissipations due to transmission bearings [44] were modelled, but not reported in the FBDs of Figure 3.

2.2.3. Vehicle and Wheels

The vehicle model considers the longitudinal dynamics and load transfer caused by the vehicle acceleration a_x , which is computed from the equilibrium equation—reported in Equation (7)—of the forces acting on the vehicle, i.e., the longitudinal forces on the tyres $F_{x,FL}, F_{x,FR}, F_{x,RL}, F_{x,RR}$, where the subscripts FL, FR, RL, RR refer to the front-left,

front-right, rear-left and rear-right wheels, respectively, the aerodynamic force F_a and the resistance force F_i due to the road slope angle α .

$$a_x = \frac{\sum_n^4 F_{x,n} - F_a - F_i}{M_v} \tag{7}$$

The term $\sum_n^4 F_{x,n}$ —where the subscript n refers to the FL, FR, RL, RR wheels—sums all the longitudinal forces on the four wheels, while the two terms F_a and F_i are as described by Equation (8):

$$\begin{cases} F_a = 0.5 \rho S_v C_d V^2 \\ F_i = M_v g \sin \alpha \end{cases} \tag{8}$$

Regarding the aerodynamic terms, ρ is the air density, S_v is the vehicle front area, C_d is the aerodynamic drag coefficient, and V is the vehicle speed. Moreover, each tyre is described by an additional degree of freedom, and since vehicle lateral dynamics are not taken into account, the angular accelerations $\ddot{\theta}_F$ and $\ddot{\theta}_R$ are the same for the two wheels at the front and rear axles, and are computed according to Equation (9):

$$\begin{cases} \ddot{\theta}_F = \frac{-T_{b,F} - F_{x,F} R_w - T_{r,F}}{J_{w,F}} \\ \ddot{\theta}_R = \frac{T_w - T_{b,R} - F_{x,R} R_w - T_{r,R}}{J_{w,R}} \end{cases} \tag{9}$$

where $T_w = T_{ds,L/R}$ is the wheel torque coming from the half shaft—which participates only for the rear wheels— $T_{b,F}$ and $T_{b,R}$ are the braking torques, and $T_{r,n}$ ($T_{r,F}$ for the front and $T_{r,R}$ for the rear) is the rolling resistance torque, which has a quadratic relationship to the wheels' rotational speed θ_n , according to Equation (10):

$$T_{r,n} = F_{z,n} R_w (f + K \dot{\theta}_n^2) \tag{10}$$

The terms f and K are the constant and quadratic coefficients of the rolling resistance and $F_{z,n}$ is the vertical load on each wheel, which is computed considering the static load distribution between the two axles—by means of parameter γ —and the dynamic load transfer due to vehicle longitudinal acceleration, using Equation (11):

$$\begin{cases} F_{z,F} = \frac{m g \gamma}{2} - \frac{m h_G a_x}{2 L} \\ F_{z,R} = \frac{m g (1-\gamma)}{2} + \frac{m h_G a_x}{2 L} \end{cases} \tag{11}$$

where L is the vehicle wheelbase and h_G is the height of the vehicle's centre of mass, whereas $F_{z,F}$ and $F_{z,R}$ indicate the vertical load on the front and rear wheels, respectively. For each wheel, the longitudinal tyre slip is computed using Equation (12):

$$\sigma = \frac{\omega R_w - V}{\omega R_w} \tag{12}$$

For sake of simplicity, the tyre model assumes a constant relaxation length L_t , even if—for more accurate results—it should be considered dependent on the vertical load and longitudinal slip [26]. Introducing the relaxation length, it is possible to correct the tyre slip, obtaining a transient slip for each tyre. Finally, the Pacejka formulation was adopted in the tyre model to evaluate the longitudinal force $F_{x,n}$ on each tyre, as a function of the different constant Pacejka parameters and three main dynamic quantities:

$$F_{x,n} = f(F_{z,n}, \mu, \sigma) \tag{13}$$

where μ is the tyre–road friction coefficient.

2.2.4. NOx Modelling

As proposed in [14], the NOx emissions were modelled considering the transient dynamics of the ICE. It has been experimentally proven that, in case of sudden acceleration by the driver, there is a spike in NOx emissions—which is expected to be 80% higher than the steady state value. Thus, in the Simulink model, a transfer function of the second order was adopted with a variable gain with respect to the engine torque T_{ICE} . The NOx emissions were estimated using the transfer function reported in Equation (14):

$$NO_X(s) = G(T_{ICE}(s)) H(s) T_e(s) \tag{14}$$

where $G(T_{ICE}(s))$ is a variable gain between the steady state NOx and the engine torque, while the second order transfer function $H(s)$ is defined as:

$$H(s) = \frac{\omega_n^2}{s^2 + 2\zeta\omega_n s + \omega_n^2} \tag{15}$$

where ω_n and ζ have been properly tuned to reproduce the transient dynamics relationship between the NOx emissions and the engine torque proposed by [14]. The NOx model here adopted takes into account only the engine-out emissions, without considering an after-treatment system device.

3. Closed Loop Control System

In this paper, the torque allocation control logic was designed to improve the vehicle drivability, to damp driveline oscillations, and to reduce engine emissions. The schematic diagram of the control strategy is reported in Figure 6. The total torque requested by the high-level part of the control logic T_e was obtained using the FeedForward (FF) contribution $T_{e,FF}$, supported by the FeedBack (FB) intervention $T_{e,FB}$. The total torque was then elaborated by the control allocation strategy (low level) to split the contribution between the engine T_{ICE} and the electric motor T_{EM} that were the input for the nonlinear model described in the previous section.

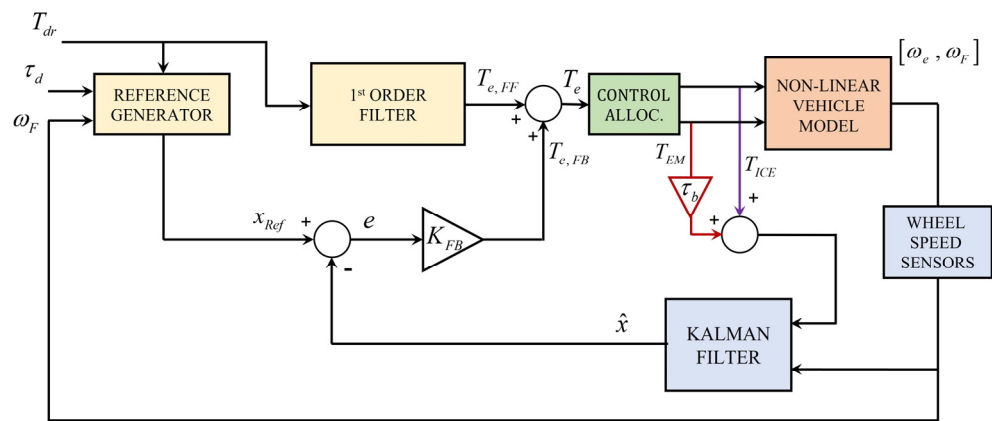


Figure 6. Driver control allocation control scheme.

3.1. High-Level Control Strategy

The gas pedal position (GPP) imposed by the driver was converted into a requested torque T_{dr} through the steady-state engine map in Figure 4 and then filtered out with a cut-off frequency of 2 Hz to elaborate the FF contribution $T_{e,FF}$.

The FB terms were designed based on a five-state linearised model, whose state space representation was defined according to the methodology presented in [11], where the effect of the torsional damper and load transfers was neglected with respect to the nonlinear model:

$$\{\dot{x}\} = [A]\{x\} + [B_1]v + [H] \tag{16}$$

where $v = T_e$ is the control output and $\{x\}$ is the state vector, composed as follows:

$$\{x\} = [x_1 \ x_2 \ x_3 \ x_4 \ x_5]^T = \left[\frac{\theta_p}{\tau_d} - \theta_R \ \dot{\theta}_R \ \dot{\theta}_p \ \dot{\theta}_F \ T_t \right]^T \tag{17}$$

where $T_t = (F_{x,RL} + F_{x,RR}) R_w$ is the steady-state driven wheel torque. Matrices $[A]$, $[B]$, and $[H]$ are described in [11]. The coordinate system of the state-space in Equation (16) is converted from the state vector $\{x\}$ of the error dynamics representation, as follows:

$$\{\dot{e}\} = [A]\{e\} + [B_1]\{v'\} \tag{18}$$

where $\{e\} = \{x_{Ref}\} - \{x\}$ and $v' = T_{e,FF} - v$, with $\{x_{Ref}\}$ represents the reference state vector, which is elaborated from the driver requested torque T_{dr} :

$$\{x_{Ref}\} = \left[\frac{T_{dr}\tau_d}{k_s} \ \dot{\theta}_{Ref} \ \dot{\theta}_{Ref}\tau_d \ \ddot{\theta}_{Ref} \ T_{dr}\tau_d \right]^T \tag{19}$$

The reference wheel speed $\dot{\theta}_{Ref}$ is obtained by integrating the reference acceleration $\ddot{\theta}_{Ref}$, defined based on the driver’s intention (T_{dr} and τ_d), and the measured wheel speed $\dot{\theta}_{F,m}$:

$$\ddot{\theta}_{Ref} = \frac{T_{dr}\eta_d\tau_d - 0.5 \rho S_v C_d (\dot{\theta}_{F,m}R_w)^2 R_w - M_v g(f + K \dot{\theta}_{F,m}^2) R_w}{(J_{w,F} + J_{w,R} + M_v R_w^2 + J_e \eta_d \tau_d^2)} \tag{20}$$

The measured wheel speed $\dot{\theta}_{F,m}$, as mentioned in Section 2, was obtained using simulated sensor dynamics that introduced a communication time delay and the digitalization of the continuous measurement signal (zero order hold technique).

The FB torque contribution was then calculated as a full state feedback law:

$$v' = -[K_{FB}]\{e\} \tag{21}$$

where the feedback gains, saved in $[K_{FB}]$, are elaborated based on the LQR design—as proposed in [35,36]. The LQR control allowed the asymptotical stability of the closed loop system and the minimisation of the quadratic performance functional J :

$$J = \int_0^\infty (\{e\}^T [Q] \{e\} + r v'^2) dt \tag{22}$$

where $[Q] = \text{diag}(1e - 9 \ 1 \ 1/\tau_d^2 \ 1 \ 1e - 9)$ is a diagonal weighted matrix where the elements relative to angular speeds are emphasized with respect to the other states.

Finally, the feedback matrix $[K_{FB}]$ was obtained as:

$$[K_{FB}] = r^{-1} [B_1]^T [P] \tag{23}$$

where P is the solution of the algebraic Riccati equation.

The total requested torque was then formulated as:

$$T_e = v = T_{e,FF} - v' = T_{e,FF} + [K_{FB}]\{e\} \tag{24}$$

To implement a full state feedback controller, a Kalman filter was also designed to estimate the state vector \hat{x} , based on the inputs of the nonlinear vehicle model v and on its measured vector y .

$$\{y\} = [\omega_e \ \omega_F] = [C]\{x\} \tag{25}$$

where $[C] = [0 \ 0 \ 1 \ 0 \ 0; 0 \ 0 \ 0 \ 1 \ 0]$ is the output matrix.

3.2. Control Allocation

The total torque T_e was then split between the ICE and the EM by the control allocation strategy. In this paper, the ICE provided the main torque contribution and the EM only intervened to compensate for the dynamic limits of the engine, e.g., when the driver requested a sudden torque through the GPP. The scheme of the control allocation strategy is reported in Figure 7.

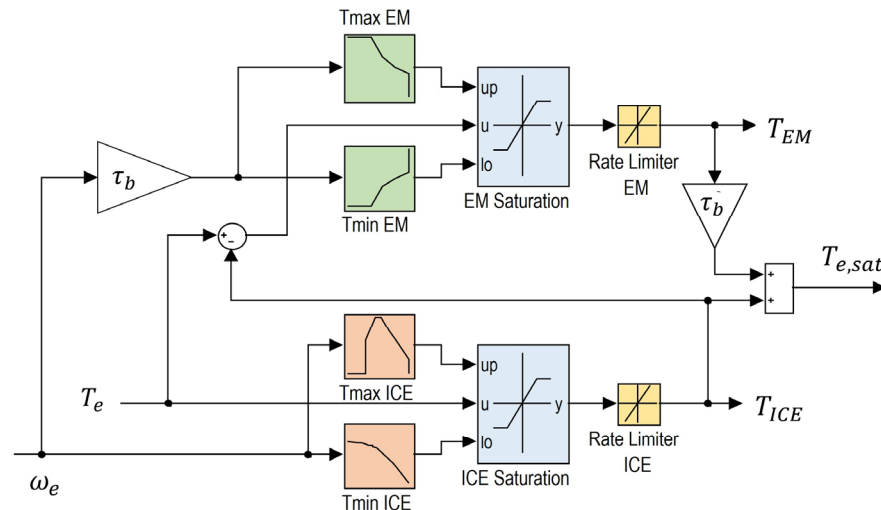


Figure 7. Control effort distribution between the ICE and EM, according to the dynamic limits of the engine.

As explained by several authors [14–16], the dynamic performance of the ICE is usually limited to reduce the engine emissions that may occur in presence of extremely dynamic torque requests. To accomplish the same task, a rate limiter was introduced into the control allocation strategy to saturate the maximum torque rate of the engine. Therefore, the torque of the EM, T_{EM} , is given by the difference between the total torque request T_e and the output torque requested to the ICE. As indicated in the scheme, the EM torque request is limited by a rate limiter, which was set at a higher level with respect to the ICE rate limiter.

In order to obtain the full benefits achieved by the methodology proposed in this paper, the energy stored in the battery should be sufficient to guarantee the requested activation of the electric motor. This energy management strategy is responsible for storing energy in the battery when the engine is more efficient, with lower polluting emissions. To exploit the benefits of this methodology, a more comprehensive design for the energy management system is required, but this is out of the scope of this paper.

4. Results

The torque allocation control designed in the previous section was finally applied to the nonlinear model described in Section 2 in order to evaluate its reference tracking performance, torque split efficacy between the ICE and the EM, and its influence on NOx emissions.

4.1. Reference Tracking Performance

The main purpose of the torque allocation control is to satisfy drivers’ requests in terms of vehicle longitudinal acceleration. The driver’s intention, expressed in terms of a reference longitudinal acceleration $a_{x,ref} = \ddot{\theta}_{Ref} R_w$, is converted into a total torque request T_e , which is obtained by the sum of the FF and FB contributions. The simulation results obtained during a tip-in manoeuvre—i.e., an instantaneous wheel torque request—are shown in Figures 8 and 9, where the influence of the two controller contributions is highlighted.

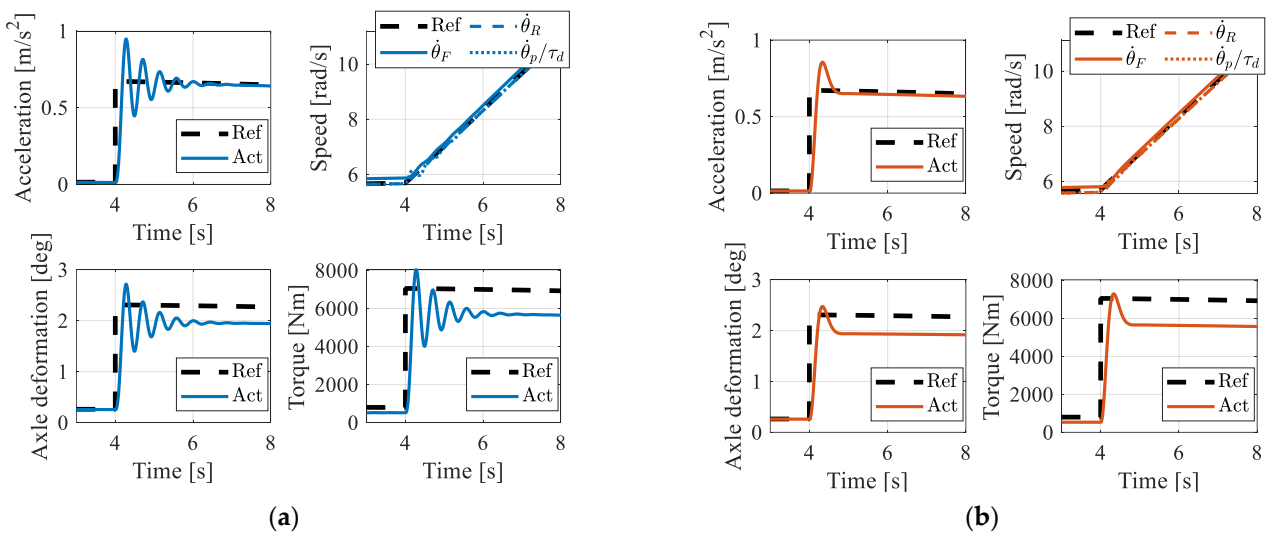


Figure 8. Vehicle state tracking performance during a tip-in manoeuvre with only the FF torque contribution (a) and with FF + FB integration (b): longitudinal acceleration (top left), front wheels, rear wheels, and primary shaft speeds (top right), rear axle deformation (down left) and torque T_t .

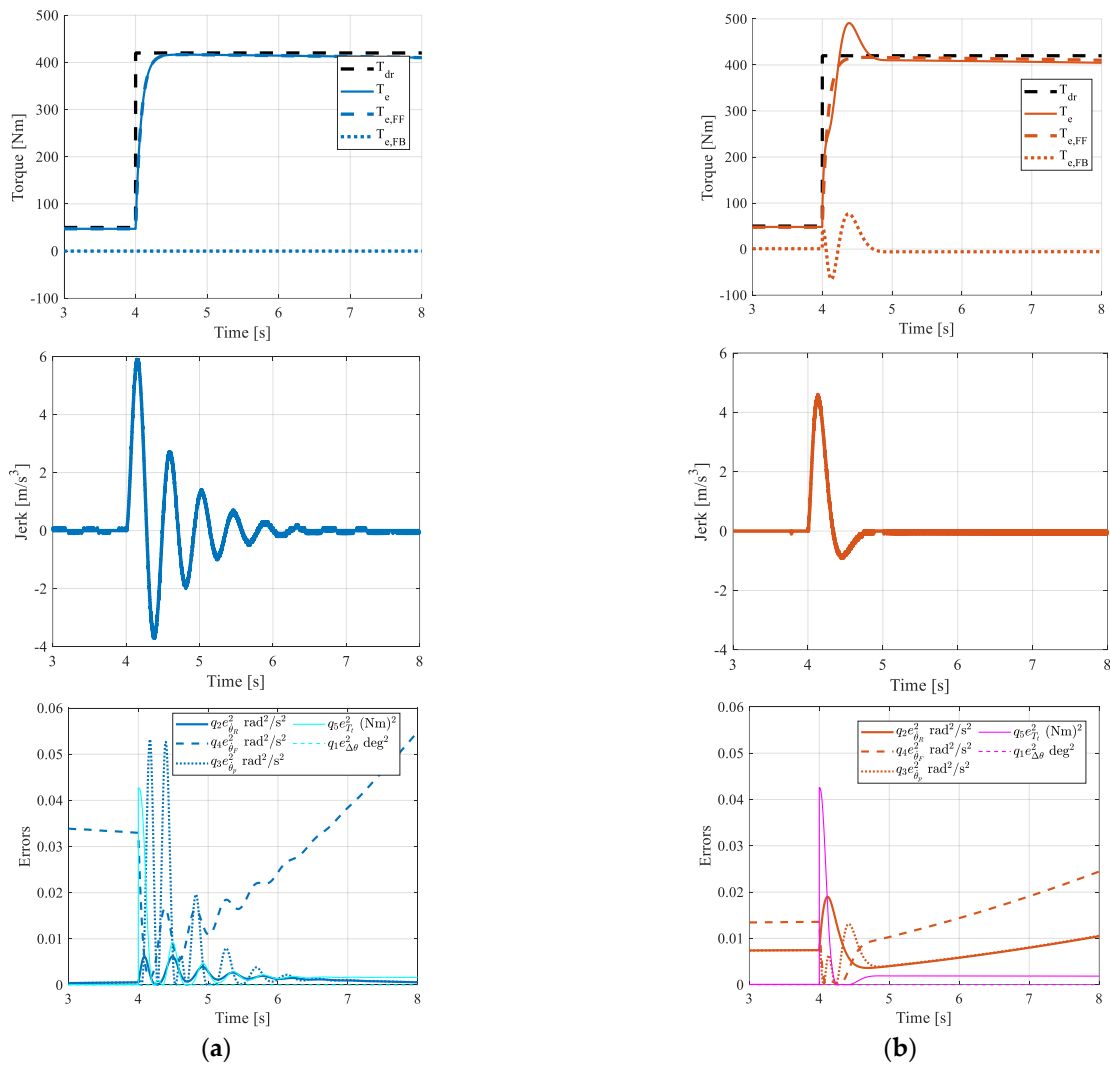


Figure 9. Control torque request (top), jerk (centre) and weighted states errors (down) during a tip-in manoeuvre with only the FF torque contribution (a) and with FF + FB integration (b).

The control, with and without the activation of the FB contribution, provided a satisfactory reference tracking performance for the speed states. However, the presence of the FB contribution improved the transient vehicle response, with an evident oscillation reduction for the whole set of states. This also implies a considerable improvement in vehicle acceleration performance and in the consequent amplitude of the corresponding jerk (i.e., derivative of the vehicle acceleration), with beneficial implications for vehicle comfort. The advantages provided by the FB integration were paid off with a peak torque request of about 20% higher than that of controller with only the FF term activated.

The FB intervention also represented a fundamental contribution to the rejection of external disturbances that may affect controller tracking performance. Indeed, the FF formulation was based on the simplified linear model, and did not include motion resistance increments due to sudden road slopes. The influence of step disturbances on the road slope is analysed in Figure 10.

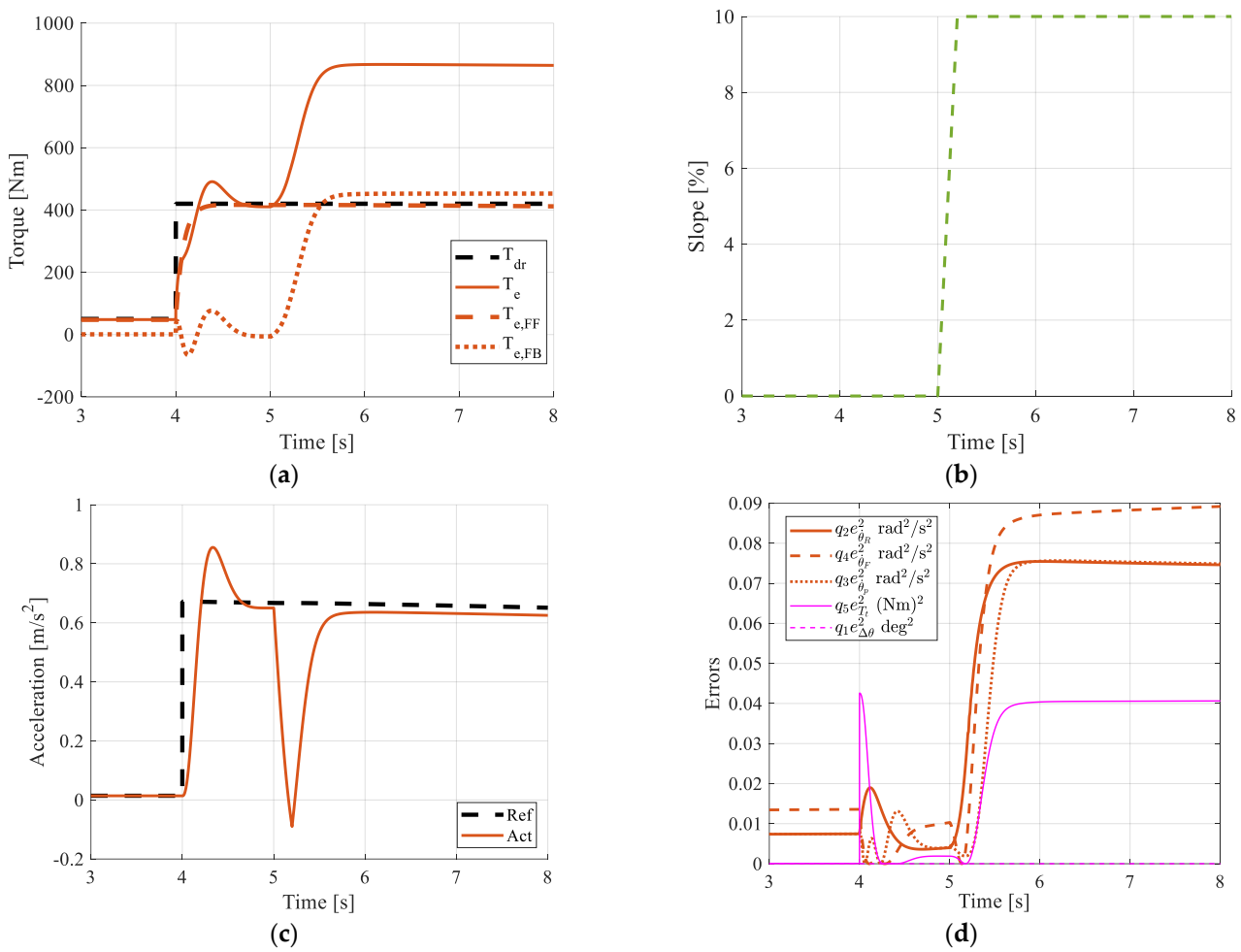


Figure 10. Control torque request (a), road slope (b), longitudinal acceleration (c) and weighted states errors (d) during a tip-in manoeuvre with the FF + FB controller mode.

The application of the torque requested by only the FF term would compromise the desired performance of the torque controller if external disturbances or uncertain/unmodelled dynamics affected the vehicle dynamics. Indeed, the FF formulation did not include the influence of the road slope, since this is a quantity that is difficult to measure or estimate—thus not representing a suitable input for feeding into a control logic. For this reason, the intervention of the FB term is essential to compensate for the higher vehicle motion resistance by applying an additional torque contribution that is able to bring the longitudinal acceleration back to the reference value; this was automatically achieved

with an acceptable worsening of state errors and without any information related to the road profile.

The effect of the FB contribution was, however, influenced by the design of the LQR cost function and the selection of the weights q_i and r . The optimal control theory [35,36] suggests that the ratio q_i/r is responsible for the trade-off between reference tracking performance and energy consumption. A sensitivity analysis of the weight r on the torque controller performance is shown in Figure 11.

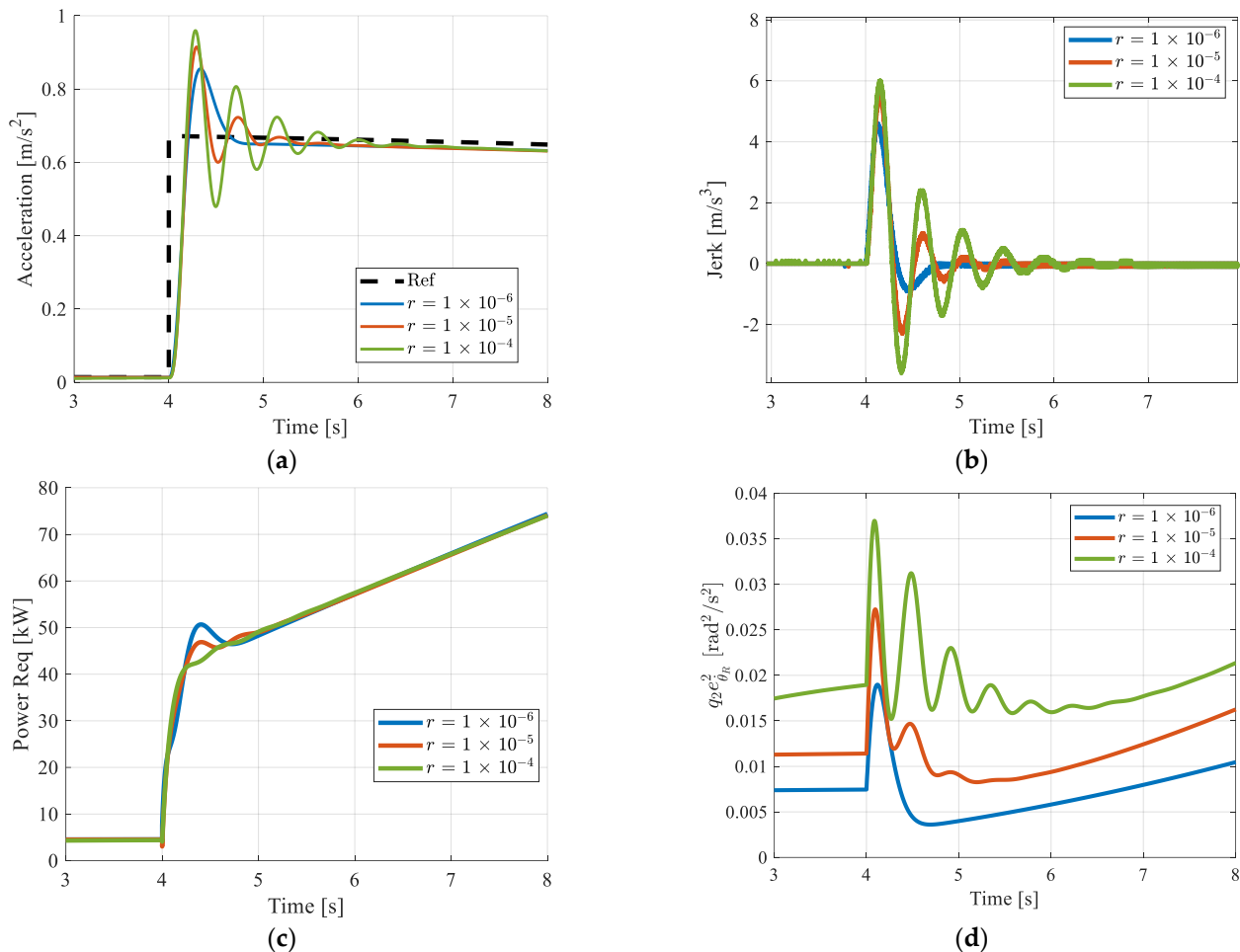


Figure 11. Vehicle acceleration (a), jerk (b), total power requested (c) and weighted rear speed error (d) during a tip-in manoeuvre with different r weights.

For low r values, the FB contribution aims at improving the reference tracking performance by reducing state errors and the amplitude of the vehicle acceleration and jerk oscillations. This advantage is obtained with a transient peak power request, i.e., the product $T_e \dot{\theta}_e$ of the engine and the electric motor. Vice versa, an increment of r would save more energy by reducing the total power request, but with an evident decline in terms of vehicle performance and comfort.

4.2. Control Allocation Evaluation

The previous section focused attention on the performance of the FF + FB controller in order to ascertain a reference total torque T_e that is able to dampen oscillations in vehicle acceleration, even in the presence of external disturbances, e.g., a road slope. However, the torque controller is not designed to take into account the powertrain’s limits in terms of engine/electric motor torque saturation and dynamic constraints. Indeed, the ICE is usually operated at low frequency dynamics to reduce combustion emissions when a steep torque

is requested, e.g., during a tip-in manoeuvre. The presence of a redundant driving source, i.e., the EM, allows the ICE's limitations to be overcome in terms of combustion emissions without compromising the vehicle's drivability. To evaluate the influence of ICE dynamics on the torque controller performance, a sensitivity analysis of the ICE rate limiter (see the scheme in Figure 7) is reported via the simulation results shown in Figures 12 and 13.

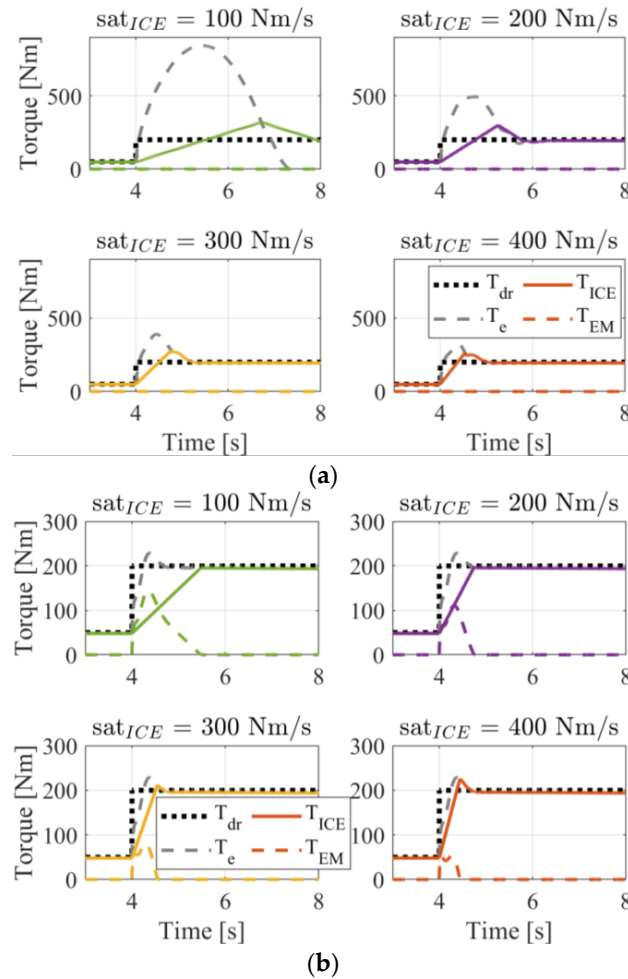


Figure 12. Torque split during a tip-in manoeuvre with only the ICE (a) and with a hybrid configuration (b) for different constraints on the ICE torque slope saturation.

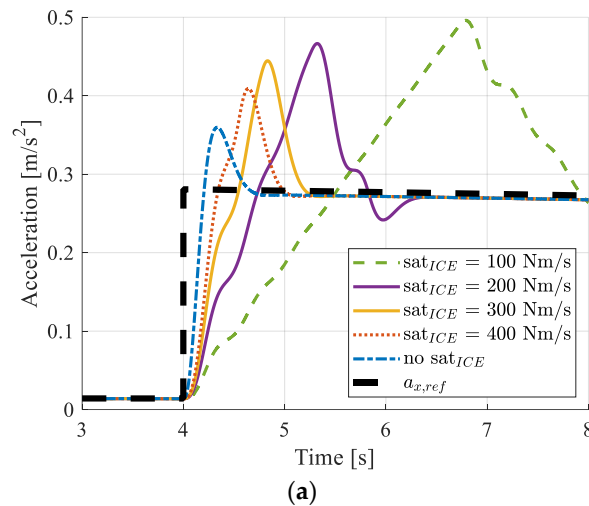


Figure 13. Cont.

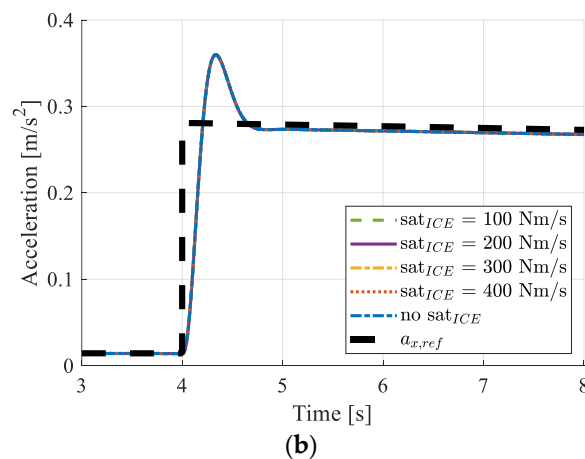


Figure 13. Longitudinal acceleration during a tip-in manoeuvre with only the ICE (a) and with a hybrid configuration (b) for different constraints on the ICE torque slope saturation.

The results presented in Figure 13a show how the dynamics of vehicle acceleration are affected by the rate limitation on the ICE-requested torque T_{ICE} . The lower the rate constraint on the T_{ICE} , the higher the overshoot and the rising time of the acceleration. These results are well explained, as the rate saturation on the torque requested by the ICE drastically influences the total torque T_e —see Figure 12a—demanded by the controller, which acts in order to reduce the states errors and so the acceleration error. The presence of an electric machine, with a typically faster response and lower emission issues than a combustion engine, allows the ICE to operate at lower frequency dynamics—thus achieving the desired performance in terms of vehicle acceleration, as shown in Figure 13b. The performance of the hybrid configuration is totally unaffected by limitations on the engine torque rate.

An important consequence of the results presented in Figures 12 and 13 is that the redundancy of power sources can also produce effective advantages in terms of the NOx emitted by the ICE. Indeed, assuming that the correlation between NOx emissions and the ICE output torque is expressed by Equation (15) [14], the benefits of reduced ICE dynamics are reported in Figure 14.

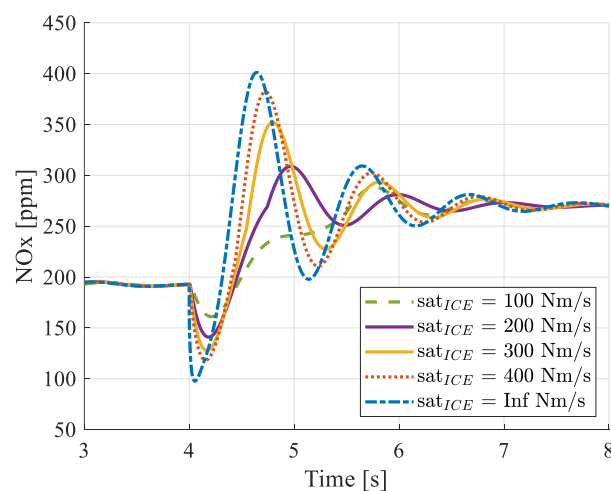


Figure 14. NOx emissions during a tip-in manoeuvre with the hybrid configuration for different constraints on the ICE torque slope saturation.

The hybrid configuration is then able to achieve the desired drivability performance, with a reduction of almost 80% in the transient NOx overshoot peak for the case of a 100 Nm/s torque rate saturation.

5. Conclusions

The paper presents a methodology for designing a torque allocation control strategy aiming at improving vehicle performance and NO_x emissions. The results obtained can be summarized in the following final remarks:

- The high level of the torque control logic generated a total torque demand that satisfied the performance requirements in terms of vehicle speed and acceleration. Both the FF and FB contributions were designed based on a simplified version of the more accurate non-linear model. The FB contribution was fundamental in improving the vehicle's transient response, damping the acceleration and jerk oscillations. Differing calibrations of the FB gains can cope with different trade-offs between state error tracking performance and the power required to minimize errors;
- The paper also showed how the FB contribution was effective in rejecting external disturbances, e.g., the road slope, by compensating for the FF contribution with an additional contribution—thus satisfying the desired reference tracking performance;
- The control allocation strategy proved to produce a satisfactory vehicle drivability performance, even in the presence of tighter constraints in the ICE torque rate. The hybrid architecture showed outstanding robustness properties against variations in the ICE torque rate when compared to the ICE-only configuration. The redundancy offered by the fast dynamics of an electric machine represents an effective way of establishing the best combination between emissions and dynamic performance.

The results confirmed the methodology's efficacy for vehicle drivability performance and engine-out emissions. However, there is still potential scope for exploring the impact of the torque control strategy on other important features related to hybrid powertrains, e.g., energy management performance, clutch engagement, and regenerative braking benefits, which are reserved for future activities.

Author Contributions: Conceptualization, L.D., A.T., E.G. and M.V.; methodology, L.D., A.T., E.G. and M.V.; software, L.D., A.T., E.G. and M.V.; validation, L.D., A.T., E.G. and M.V.; formal analysis, L.D., A.T., E.G. and M.V.; investigation, L.D., A.T., E.G. and M.V.; writing—original draft preparation, L.D., A.T., E.G. and M.V.; writing—review and editing, L.D., A.T., E.G. and M.V.; visualization, L.D., A.T., E.G. and M.V.; supervision, E.G. and M.V. All authors have read and agreed to the published version of the manuscript.

Funding: This research received no external funding.

Institutional Review Board Statement: Not applicable.

Informed Consent Statement: Not applicable.

Data Availability Statement: Not applicable.

Conflicts of Interest: The authors declare no conflict of interest.

References

1. Awadallah, M.; Tawadros, P.; Walker, P.; Zhang, N. Comparative fuel economy, cost and emissions analysis of a novel mild hybrid and conventional vehicles. *Proc. IMechE Part D J. Automob. Eng.* **2018**, *232*, 1846–1862. [[CrossRef](#)]
2. Emadi, A.; Rajashekara, K.; Williamson, S.S.; Lukic, S.M. Topological overview of hybrid electric and fuel cell vehicular power system architectures and configurations. *IEEE Trans. Veh. Technol.* **2005**, *54*, 763–770. [[CrossRef](#)]
3. Sciarretta, A.; Back, M.; Guzzella, L. Optimal control of parallel hybrid electric vehicles. *IEEE Trans. Control Syst. Technol.* **2004**, *12*, 352–363. [[CrossRef](#)]
4. Barsali, S.; Miulli, C.; Possenti, A. A control strategy to minimize fuel consumption of series hybrid electric vehicles. *IEEE Trans. Energy Convers.* **2004**, *19*, 187–195. [[CrossRef](#)]
5. Castellano, A.; Cammalleri, M. Power losses minimization for optimal operating maps in power-split HEVs: A case study on the Chevrolet Volt. *Appl. Sci.* **2021**, *11*, 7779. [[CrossRef](#)]
6. Tota, A.; Galvagno, E.; Velardocchia, M. On the power-weighted efficiency of multimode powertrains: A case study on a two-mode hybrid system. In *I4SDG 2021, Proceedings of the 1st Workshop IFToMM for Sustainable Development Goals, Mechanisms and Machine Science, Online, 25–26 November 2021*; Quaglia, G., Gasparetto, A., Petuya, V., Carbone, G., Eds.; Springer: Cham, Switzerland, 2022; Volume 108, pp. 522–531. [[CrossRef](#)]

7. Tota, A.; Galvagno, E.; Dimauro, L.; Vigliani, A.; Velardocchia, M. Energy management strategy for hybrid multimode powertrains: Influence of inertial properties and road inclination. *Appl. Sci.* **2021**, *11*, 11752. [[CrossRef](#)]
8. Mantriota, G.; Reina, G.; Ugenti, A. Performance evaluation of a compound power-split CVT for hybrid powertrains. *Appl. Sci.* **2021**, *11*, 8749. [[CrossRef](#)]
9. Cirimele, V.; Dimauro, L.; Repetto, M.; Bonisoli, E. Multi-objective optimisation of a magnetic gear for powertrain applications. *Int. J. Appl. Electromagn. Mech.* **2019**, *60*, S25–S34. [[CrossRef](#)]
10. Nazari, S.; Siegel, J.; Stefanopoulou, A. Optimal energy management for a mild hybrid vehicle with electric and hybrid engine boosting systems. *IEEE Trans. Veh. Technol.* **2019**, *68*, 3386–3399. [[CrossRef](#)]
11. Galvagno, E.; Velardocchia, M.; Vigliani, A. Drivability enhancement and transient emission reduction for a mild hybrid diesel-electric truck. *Int. J. Powertrains* **2013**, *2*, 262–291. [[CrossRef](#)]
12. Parmar, V.; Di Rocco, D.; Sopouch, M.; Albertini, P. Multi-physics simulation model for noise and vibration effects in hybrid vehicle powertrain. *SAE Tech. Pap.* **2014**, 2014-01-2093. [[CrossRef](#)]
13. Chen, J.-S.; Hwang, H.-Y. Engine automatic start–stop dynamic analysis and vibration reduction for a two-mode hybrid vehicle. *Proc. IMechE Part D J. Automob. Eng.* **2013**, *227*, 1303–1312. [[CrossRef](#)]
14. Hagen, J.R.; Filipi, Z.S.; Assanis, D.N. Transient diesel emissions: Analysis of engine operation during a tip-in. *SAE Tech. Pap.* **2006**, 2006-01-1151. [[CrossRef](#)]
15. Wüst, M.; Krüger, M.; Naber, D.; Cross, L.; Greis, A.; Lachenmaier, S.; Stotz, I. Operating strategy for optimized CO₂ and NO_x emissions of diesel-engine mild-hybrid vehicles. In Proceedings of the 15. Internationales Stuttgarter Symposium: Automobil- und Motorentechnik, Stuttgart, Germany, 17–18 March 2015; Springer: Wiesbaden, Germany, 2015. [[CrossRef](#)]
16. Thibault, L.; Sciarretta, A.; Degeilh, P. Reduction of pollutant emissions of diesel mild hybrid vehicles with an innovative energy management strategy. In Proceedings of the 2017 IEEE Intelligent Vehicles Symposium (IV), Los Angeles, CA, USA, 11–14 June 2017; pp. 1274–1279. [[CrossRef](#)]
17. Le Guen, D.; Weck, T.; Balihe, A.; Verbeke, B. Definition of gearshift pattern: Innovative optimization procedures using system simulation. *SAE Int. J. Engines* **2011**, *4*, 412–431. [[CrossRef](#)]
18. Pramanik, S.; Anwar, S. Predictive optimal control of mild hybrid trucks. *Vehicles* **2022**, *4*, 71. [[CrossRef](#)]
19. Guercioni, G.R.; Galvagno, E.; Tota, A.; Vigliani, A. Adaptive equivalent consumption minimization strategy with rule-based gear selection for the energy management of hybrid electric vehicles equipped with dual clutch transmissions. *IEEE Access* **2020**, *8*, 190017–190038. [[CrossRef](#)]
20. Farshidianfar, A.; Ebrahimi, M.; Bartlett, H. Hybrid modelling and simulation of the torsional vibration of vehicle driveline systems. *Proc. IMechE Part D J. Automob. Eng.* **2001**, *215*, 217–229. [[CrossRef](#)]
21. Galvagno, E.; Dimauro, L.; Mari, G.; Velardocchia, M.; Vella, A.D. Dual Clutch Transmission vibrations during gear shift: A simulation-based approach for clunking noise assessment. *SAE Tech. Pap.* **2019**, 2019-01-1553. [[CrossRef](#)]
22. Galvagno, E.; Guercioni, G.R.; Vigliani, A. Sensitivity analysis of the design parameters of a Dual-Clutch Transmission focused on NVH performance. *SAE Tech. Pap.* **2016**, 2016-01-1127. [[CrossRef](#)]
23. Awadallah, M.; Tawadros, P.; Walker, P.; Zhang, N. Dynamic modelling and simulation of a manual transmission based mild hybrid vehicle. *Mech. Mach. Theory* **2017**, *112*, 218–239. [[CrossRef](#)]
24. Guzzomi, A.L.; Sharman, A.; Stone, B.J. Some torsional stiffness and damping characteristics of a small pneumatic tyre and the implications for powertrain dynamics. *Proc. IMechE Part D J. Automob. Eng.* **2010**, *224*, 229–244. [[CrossRef](#)]
25. Bartram, M.; Mavros, G.; Biggs, S. A study on the effect of road friction on driveline vibrations. *Proc. IMechE Part K J. Multi-Body Dyn.* **2010**, *224*, 321–340. [[CrossRef](#)]
26. Rill, G. First order tyre dynamics. In Proceedings of the III European Conference on Computational Mechanics, Solids, Structures and Coupled Problems in Engineering, Lisbon, Portugal, 5–8 June 2006. [[CrossRef](#)]
27. Dolcini, P.J.; Canudas-de-Wit, C.; Béchart, H. *Dry Clutch Control for Automotive Applications*, 1st ed.; Springer: London, UK, 2010; pp. 1–144.
28. Canudas-de-Wit, C.; Tsiotras, P.; Velenis, E.; Basset, M.; Gissing, G. Dynamic Friction Models for Road/tyre Longitudinal Interaction. *Veh. Syst. Dyn.* **2003**, *39*, 189–226. [[CrossRef](#)]
29. Rovarino, D.; Actis Comino, L.; Bonisoli, E.; Rosso, C.; Venturini, S.; Velardocchia, M.; Baecker, M.; Gallrein, A. Hardware and virtual test-rigs for automotive steel wheels design. *SAE Int. J. Adv. Curr. Prac. Mobil.* **2020**, *2*, 3481–3489. [[CrossRef](#)]
30. Friedriksson, J. Improved driveability of a hybrid electric vehicle using powertrain control. *Int. J. Altern. Propuls.* **2006**, *1*, 97–111. [[CrossRef](#)]
31. Ito, Y.; Tomura, S.; Moriya, K. Development of vibration reduction motor control for hybrid vehicles. In Proceedings of the IECON 2007—33rd Annual Conference of the IEEE Industrial Electronics Society, Taipei, Taiwan, 5–8 November 2007; pp. 516–521. [[CrossRef](#)]
32. Baumann, J.; Torkzadeh, D.D.; Ramstein, A.; Kiencke, U.; Schlegl, T. Model-based predictive anti-jerk control. *Control Eng. Pract.* **2006**, *14*, 259–266. [[CrossRef](#)]
33. Filippini, M.; Torchio, R.; Alotto, P.; Bonisoli, E.; Dimauro, L.; Repetto, M. A new class of devices: Magnetic gear differentials for vehicle drivetrains. *IEEE Trans. Transp. Electrification* **2022**. [[CrossRef](#)]
34. Berriri, M.; Chevrel, P.; Lefebvre, D. Active damping of automotive powertrain oscillations by a partial torque compensator. *Control Eng. Pract.* **2008**, *16*, 874–883. [[CrossRef](#)]

35. Anderson, B.D.O.; Moore, J.B. *Optimal Control: Linear Quadratic Methods*, 1st ed.; Prentice-Hall: Englewood Cliffs, NJ, USA, 1990.
36. Ostertag, E. *Mono- and Multivariable Control and Estimation: Linear, Quadratic and LMI Methods*; Springer: Berlin/Heidelberg, Germany, 2011.
37. Venturini, S.; Bonisoli, E. Design of a spherical pendulum didactic test rig. *Int. J. Mech. Control* **2018**, *19*, 69–76.
38. Walters, J.E.; Krefta, R.J.; Gallegos-Lopes, G.; Fattic, G.T. Technology considerations for belt alternator starter systems. *SAE Tech. Pap.* **2004**, 2004-01-0566. [[CrossRef](#)]
39. Morra, E.; Spessa, E.; Ciaravino, C.; Vassallo, A. Analysis of various operating strategies for a parallel-hybrid diesel powertrain with a belt alternator starter. *SAE Int. J. Altern. Powertrains* **2012**, *1*, 231–239. [[CrossRef](#)]
40. Auerbach, M.; Ruf, M.; Bargende, M.; Reuss, H.-C.; Van Doorn, R.; Wilhelm, F.; Kutschera, I. Potentials of phlegmatization in diesel hybrid electric vehicles. *SAE Tech. Pap.* **2011**, 2011-37-0018. [[CrossRef](#)]
41. Velardocchia, M.; D’Alfio, N.; Bonisoli, E.; Galvagno, E.; Amisano, F.; Sorniotti, A. Block-oriented models of torque gap filler devices for AMT transmissions. *SAE Tech. Pap.* **2008**, 2008-01-0631. [[CrossRef](#)]
42. Dimauro, L.; Bonisoli, E.; Repetto, M. Dynamic behaviour and magneto-mechanical efficiency of a contactless magnetic transmission. In *Rotating Machinery, Optical Methods & Scanning LDV Methods, Proceedings of the 40th IMAC, Orlando, FL, USA, 7–10 February 2022*; Di Maio, D., Baqersad, J., Eds.; Springer: Cham, Switzerland, 2023; Volume 6, pp. 129–138. [[CrossRef](#)]
43. Pacejka, H.B. *Tyre and Vehicle Dynamics*, 2nd ed.; Butterworth: Oxford, UK, 2005; pp. 1–621.
44. Sorniotti, A.; Sampò, E.; Velardocchia, M.; Bonisoli, E.; Galvagno, E. Friction inside wheel hub bearings: Evaluation through analytical models and experimental methodologies. *SAE 2007 Trans. J. Engines* **2007**, *116*, 1665–1676. [[CrossRef](#)]

Disclaimer/Publisher’s Note: The statements, opinions and data contained in all publications are solely those of the individual author(s) and contributor(s) and not of MDPI and/or the editor(s). MDPI and/or the editor(s) disclaim responsibility for any injury to people or property resulting from any ideas, methods, instructions or products referred to in the content.